THE JOURNAL OF PHYSICAL CHEMISTRY B
A JOURNAL OF THE AMERICAN CHEMICAL SOCIETY

pubs.acs.org/JPCB

Article

Interactions of Curcumin's Degradation Products with the Aβ_{42} Dimer: A Computational Study

Maryam Haji Dehabadi, Amedeo Caflisch, Ioana M. Ilie,* and Rohoullah Firouzi*

Cite This: J. Phys. Chem. B 2022, 126, 7627−7637

Read Online

ACCESS | Metrics & More | Article Recommendations | Supporting Information

ABSTRACT: Amyloid-β (Aβ) dimers are the smallest toxic species along the amyloid-aggregation pathway and among the most populated oligomeric accumulations present in the brain affected by Alzheimer's disease (AD). A proposed therapeutic strategy to avoid the aggregation of Aβ into higher-order structures is to develop molecules that inhibit the early stages of aggregation, i.e., dimerization. Under physiological conditions, the Aβ dimer is highly dynamic and does not attain a single well-defined structure but is rather characterized by an ensemble of conformations. In a recent study, a highly heterogeneous library of conformers of the Aβ dimer was generated by an efficient sampling method with constraints based on ion mobility mass spectrometry data. Here, we make use of the Aβ dimer library to study the interaction with two curcumin degradation products, ferulic aldehyde and vanillin, by molecular dynamics (MD) simulations. Ensemble docking and MD simulations are used to provide atomistic detail of the interactions between the curcumin degradation products and the Aβ dimer. The simulations show that the aromatic residues of Aβ, and in particular ^{19}FF^{20}, interact with ferulic aldehyde and vanillin through $\pi-\pi$ stacking. The binding of these small molecules induces significant changes on the ^{16}KLVFF^{20} region.

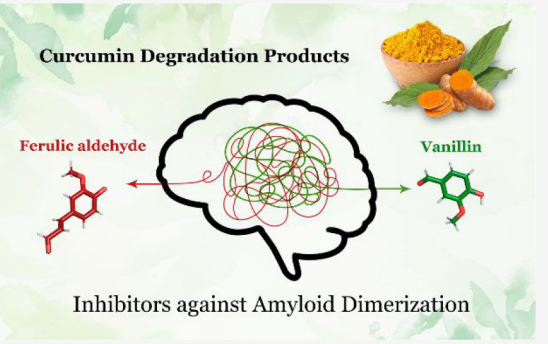

INTRODUCTION

The onset of a wide range of neurodegenerative diseases, including Parkinson's disease (PD), type 2 diabetes, and Alzheimer's disease (AD), is associated with the aggregation of intrinsically disordered proteins (IDPs).[1,2] AD is the most common neurodegenerative disease currently affecting over 50 million people worldwide and is estimated to reach 131.5 million by 2050.[3−5] There are some reasons for the failure of drug design to treat AD, and the majority of approved drugs against AD treat only the symptoms and fail to prevent or cure the onset of the disease.[6] The pathological hallmark of AD is the presence of extracellular senile plaques and intracellular neurofibrillary tangles formed from the amyloid-β peptide (Aβ) and tau protein, respectively.[7] Extracellular amyloid fibrils have been proposed to disrupt neuronal communication, while intracellular tau-containing tangles can block neuronal transport.[2,8,9]

The dominant forms of the Aβ peptide are 40 and 42 residues long, with the latter being the predominant species in amyloid plaques.[2] Structurally, the Aβ peptides consist of a disordered N-terminus (first 15 residues), a central hydrophobic cluster (CHC) spanning residues 16−21, and a hydrophobic C-terminus (last 10−12 residues).[10] Amyloid formation follows a nucleation−elongation mechanism.[11,12] Briefly, soluble monomers undergo conformational transitions and can aggregate to form dimers, trimers, or oligomers, which then evolve to form fibrillar structures.[10] Therefore, preventing or reducing the aggregation of the Aβ is an effective therapeutic strategy against AD. A variety of inhibitors, ranging from natural products, peptides, synthetic compounds, to antibodies and larger proteins have been developed to interfere with Aβ_{42} aggregation.[13−23] For instance, the monoclonal antibody aducanumab can selectively interact with Aβ_{42} aggregates, clearing the brain from amyloid plaques.[24] The structural complexity of biologics makes them susceptible to degradation, which complicates the cellular delivery process. Small molecules from natural products can be more effective at addressing intracellular targets, offer a great chemical diversity, and can be effective in the prevention and treatment of various forms of neurodegenerative diseases.[25]

Curcumin is a natural product with anticancer, antioxidant, antiviral, antifungal, anti-inflammatory, and antibacterial properties, which was proposed to have a high therapeutic potential against AD.[17,18,22,23,26−41] Structurally, its flexible backbone, its hydrophobic nature, and the availability of hydrogen bond donors and acceptors[42] make it an ideal inhibitory candidate for the amyloid-aggregation process. *In vitro* studies showed that curcumin can reduce the β-sheet

Received: August 15, 2022
Revised: September 18, 2022
Published: September 23, 2022

https://doi.org/10.1021/acs.jpcb.2c05846
J. Phys. Chem. B 2022, 126, 7627−7637

content,[31] block Aβ oligomers,[31] destabilize and reduce Aβ fibrils,[32] and also break the formed tau tangles.[33] Furthermore, *in vivo* studies indicated that curcumin can disassemble tau oligomeric species[23,34] and reduce insoluble Aβ oligomers and plaques,[35,36] which could limit the progression of AD. Curcumin was shown to have antiamyloidogenic and fibril-destabilizing effects and to promote the formation of "off-pathway" soluble oligomers and prefibrillar aggregates.[32,35,37,38] An *in vivo* study showed that curcumin injected into mice crossed the blood−brain barrier and bound to amyloid plaques.[35] Despite its beneficial properties, it has a low bioavailability and degrades easily,[43−45] which limit its clinical application. Novel curcumin formulations (longvida and theracurmin) administered in low doses (80−180 mg/day) overcome the poor *in vivo* bioavailability[39] of curcumin.[40,41] A recent study showed that oral consumption of a bioavailable form of curcumin (theracurmin) led to significant memory improvement, which was attributed to the decrease in amyloid and tau aggregations.[41] Moreover, curcumin is unstable in aqueous solution and undergoes rapid hydrolysis.[46,47] Wang et al. found that 90% of curcumin degraded into various products such as ferulic aldehyde, *trans*-6-(4′-hydroxy-3′-methoxyphenyl)-2,4-dioxo-5-hexenal, feruloyl methane, ferulic acid, and vanillin within 30 min in phosphate buffer at pH 7.4.[39] The degradation products of curcumin have a higher solubility as compared to curcumin and may therefore be appropriate candidate for anti-AD therapeutics.[46] As a matter of fact, ferulic acid can protect neurons against Aβ-induced oxidative stress, which plays a significant role in the pathology of AD.[48−53] Additionally, ferulic acid can dose-dependently prevent both formation and extension of Aβ oligomers and destabilize Aβ fibrils.[54] An *in vitro* study showed that vanillin has acetylcholinesterase inhibitory activities, leading to the restoration of acetylcholine levels in diseased brains leading to an improvement in memory function.[55] Vanillin has also been shown to prevent amyloid-aggregation *in vivo*.[56] Furthermore, vanillin derivatives have exhibited the enhanced antioxidant and antiacetylcholinesterase properties, which could be as multitarget hybrid compounds for AD treatment.[57] Vanillic acid is the oxidant form of vanillin, which can be neuroprotective against Aβ-induced neurotoxicity in the Aβ-injected mouse brain.[58,59] Hence, the therapeutic potential of curcumin against Alzheimer's disease may originate from its degradation products, which could contribute largely to its pharmacological activities.

Complementing experiments, computational studies reinforce the fact that curcumin and its products disaggregate and destabilize Aβ protofibrils and fibrils,[17,18,60−65] deform the β-sheet structure in Aβ_{42} dimers,[66] and also form numerous interactions with the Aβ monomer.[22,67,68] Salamanova et al. found that curcumin and ferulic acid increase the helical content of the Aβ_{42} peptide.[22] A recent computational study consisting of docking followed by multins MD simulations of curcumin and a hexamer peptide model of Aβ_{42} fibril showed that curcumin partly dissociates the tip peptide of the Aβ_{42} fibril by disrupting the β-sheet within the ^{12}VHHQKLVFF^{20} sequence.[60]

Here, we explore the therapeutic potential of curcumin against Alzheimer's disease, which may originate from its degradation products. We investigate the effects of ferulic aldehyde and vanillin on Aβ_{42} dimers by means of computer simulations. In a recent work, we built a diverse conformational library of the Aβ_{42} dimers using the blockwise excursion sampling (BES) and standard CHARMM force fields.[69,70] We demonstrated that the conformational library of Aβ_{42} dimers generated by the CHARMM36m force field is in good agreement with experimental data.[69] In the present study, we use the generated CHARMM36m library to identify the binding sites of the curcumin degradation products in Aβ_{42} dimers through a new computational pipeline in the framework of the ensemble docking strategy. Next, we perform MD simulations consisting of Aβ_{42} peptide−small molecule complexes to study the effects of the degradation products in a dynamic environment.

MATERIALS AND METHODS

Preparation of Aβ_{42} Dimer Library and Ligands. The library of Aβ_{42} dimers was generated using the blockwise excursion sampling (BES) protocol, which was recently employed for the construction of a diverse conformational library for Aβ_{42} monomers and dimers.[69,70] The BES protocol comprises simulating annealing and many short conventional MD simulations which are called blocks and denoted as $\mathbf{\Gamma}^{\mathbf{SA}}$ and $\mathbf{\Gamma}^{\mathbf{MD}}$, respectively. Two consecutive simulated annealing and MD simulation blocks are referred to as an SA:MD block ($\mathbf{\Gamma}^{\mathbf{SA:MD}}$), and five $\mathbf{\Gamma}^{\mathbf{SA:MD}}$ blocks with five different T_{max} values equal to 700, 600, 500, 400, and 350 K form an excursion chain (EC). T_{max} is an important parameter in the simulated annealing block which is the final temperature after the heat-up run. The protocol exploits the ability of simulated annealing to overcome high barriers in the free energy landscape. Each simulated annealing block is followed by a short MD simulation at constant temperature (310 K). The trajectories in MD simulation blocks are used for the sampling of structures. We used 1000 excursion chains (N_{EC} = 1000) and built the initial structures of extended and parallel Aβ_{42} dimers. For more details on this sampling methodology and its terminology, see refs 69 and 70. The Aβ_{42} dimer structures sampled by the BES protocol were clustered using the Daura algorithm[71] with a carbon alpha (Cα) root-mean-square deviation (RMSD) cutoff of 0.3 nm. This analysis produced 41322 clusters. Then, collision cross section (CCS) values were calculated for all structures. A total of 1183 representative structures of all MD snapshots that satisfied the experimental value of CCS (1252 ± 20 Å^2) were selected[69,72] and used as a library of Aβ_{42} dimers for the docking protocol after energy minimization by 5000 iterations of the steepest descent algorithm. The MD simulations were carried out using the GROMACS 5.1.5 software.[73,74] The CHARMM36m all-atom force field[75] and the generalized Born (GB) water model[76] were used. The structures of the two degradation products of curcumin (ferulic aldehyde and vanillin, Figure 1) were extracted from the ZINC database.[77] The GAMESS package[78] was used to optimize all ligands at the B3LYP exchange and correlation functional[79] and the 6-31+G(d,p) basis set.

Docking Setup. The curcumin degradation products were docked against all 1183 Aβ_{42} dimers in the library using

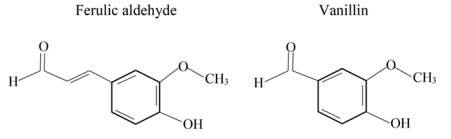

Figure 1. Chemical structure of the degradation products of curcumin used in this study.

https://doi.org/10.1021/acs.jpcb.2c05846
J. Phys. Chem. B 2022, 126, 7627−7637

AutoDock Vina (version 1.1.2).[80] The docking search space around each representative structure of the Aβ_{42} dimer was defined by a rectangular box centered at the center of mass of the Aβ_{42} dimer. The minimal distance of 1.2 nm from the Aβ_{42} dimer to the edge of the box was set. Different optimized docking boxes were defined for each system depending on the size and shape of the Aβ_{42} dimer conformation. Each docking run produced nine optimal Aβ_{42} dimer−ligand configurations, and in total 10647 (= 1183 × 9) poses were generated. The different poses for each run were ranked by the binding free energy. The top scoring pose for each run is related to the complex with the most favorable binding free energy. The other lower-ranked poses were selected since sometimes the pose with the lowest RMSD relative to the experimental pose is not captured by Vina.[19] To select the high-ranked complexes, $\Delta\Delta G_{binding}$ was defined as the difference of binding free energy between the top-ranked pose and the lower-ranked pose ($\Delta G_{toppose} - \Delta G_{lower\text{-}rankedpose}$). Different cutoff values of $\Delta\Delta G_{binding}$ (0.1, 0.2, and 0.3 kcal/mol) were used for selecting the generated docking complexes (Table 1). The results were

Table 1. Number of Selected Docking Complexes for Each Ligand with the Different $\Delta\Delta G_{binding}$ Cutoffs

$\Delta\Delta G_{binding}$ (kcal/mol)	ferulic aldehyde	vanillin
0.1	1702	1679
0.2	2895	2746
0.3	4537	4240

obtained for different cutoff values and for each ligand. The results for $\Delta\Delta G_{binding}$ cutoff values of 0.1, 0.2, and 0.3 kcal/mol can be found in the Supporting Information.

MD Simulations Setup. *System Preparation.* Two distinct sets of simulations were set up and simulated following identical protocols. First, 10 independent copies consisting of an Aβ_{42} dimer−ligand complex were selected from the highest-ranked pose extracted from docking results to investigate the stability of the complex (Figures S1 and S2 in the Supporting Information). Second, 10 independent copies starting from dimer−ligand complexes, in which the ligand was randomly placed at noninteracting distances from the dimer, were run to identify secondary interaction hot spots on the dimer surface and to investigate the effects of the small molecules on the conformations of the peptides in the presence of each ligand. The initial structure of the Aβ_{42} dimer was the most populated structure of the Aβ_{42} dimer generated by the BES protocol that has the collision cross sections in agreement with the experimental value. The parameters for all ligands were generated using the CHARMM general force field (CGenFF).[81]

Production Simulations. All simulations were carried out using the GROMACS 2020.4 package,[73,74] the CHARMM36m force field,[75] and the TIP3P water model.[82] Each system was placed in a cubic box of 9 nm per edge, and periodic boundary conditions were applied. Explicit Na^+ and Cl^- ions were added to neutralize the charge of the systems and convey a background concentration of 150 mM. Following the steepest descents minimization, the equilibration was done in the NPT ensemble with position restraints on the backbone of the Aβ_{42} dimer and the heavy atoms of the ligands. The temperature and pressure were maintained constant at 310 K and 1 atm by using the velocity-rescaling thermostat[83] and Berendsen barostat,[84] respectively. The first set of simulations, started from the top scoring pose, cumulate 600 ns per ligand (10 independent 60 ns simulations per ligand). The second set of simulations, started from random positions and orientations of the ligands, cumulates 2 μs per ligand (10 independent 200 ns simulations per ligand) in the absence of any restraints. All production simulations were started using different initial random velocities and were carried out in the NVT ensemble. The cutoff values for the van der Waals and Coulombic interactions were set to 1.2 nm. The electrostatic interactions were calculated by the particle mesh Ewald (PME) method.[85] A time step of 2 fs was employed for all simulations. Bond lengths were constrained using a fourth-order LINCS algorithm[86] with 2 iterations.

RESULTS AND DISCUSSION

We first investigated the stability of the dimer−ligand complexes starting from the highest-ranked docked poses. The analysis revealed that the ligands dissociate from the Aβ_{42} dimer within the first 30 ns. This does not come as a surprise as in the docking step the small molecule is anchored to a rigid interface, while in the MD simulations the complex is highly dynamic (Figures S3 and S4). Additionally, the conformational changes of the dimer can facilitate formation of binding sites more readily accessible by the ligand. Hence, the reattachment of the small molecule at secondary short-lived interaction sites is observed. Therefore, we performed molecular dynamics simulations starting from noninteracting distances of the small molecules from the Aβ_{42} dimer to eliminate any bias introduced by the initial pose or effects of the rigid dimer conformation. These simulations were used for the analysis. To assess the convergence of docking and MD simulations, the number of contacts between each ligand and individual residues of the two peptides forming the dimer were calculated (Figures S5 and S6 in the Supporting Information), and the results indicate that reasonable convergence has been reached.

Identifying the Binding Site of Curcumin Compounds. To identify which residues and regions interact most with the ligands, we calculated the average contact number between each Aβ_{42} residue and small molecule ligand. The results show that the segments ^{4}FRHDSGY^{10}, ^{19}FF^{20}, ^{28}KG^{29}, and ^{34}LMVGG^{38} interact most with ferulic aldehyde (Figure 2a). Similarly, vanillin interacts predominantly with residue sequences ^{9}GY^{10}, ^{19}FF^{20}, and ^{33}GLMVGG^{38} (Figure 2b). Both ligands share the interaction hot spots along the sequence of Aβ_{42} (regions of ^{19}FF^{20}, ^{34}LMVGG^{38}, and ^{9}GY^{10}), which indicates the homogeneity of the Aβ_{42} dimer molecular recognition sites across the ligands. Importantly, the hot spot regions ^{19}FF^{20} and ^{34}LMVGG^{38} are part of the central hydrophobic cluster (CHC) and the C-terminus hydrophobic region, respectively, which drive Aβ fibrillization.[87−97] In line with the contact number analysis, the analysis obtained from ensemble docking (Figures S7−S12 in the Supporting Information) indicates that the ligands attach primarily to the CHC region, particularly to its aromatic residues (F19 and F20). These observations are consistent with previous molecular dynamics simulations, which showed that curcumin forms longer lived contacts with residues I32, L34, and M35, while the aromatic residues F19 and F20 showed a high propensity to interact with the rings of curcumin.[66] Based on the fragment mapping calculations on the monomeric form of the Aβ_{42} peptide, Zhu et al. reported F4 and Y10 together with L17, F19, I31, and M35 as binding "hot spots" of curcumin in the Aβ_{42} peptide.[68] Additionally, a multiscale computational

https://doi.org/10.1021/acs.jpcb.2c05846
J. Phys. Chem. B 2022, 126, 7627−7637

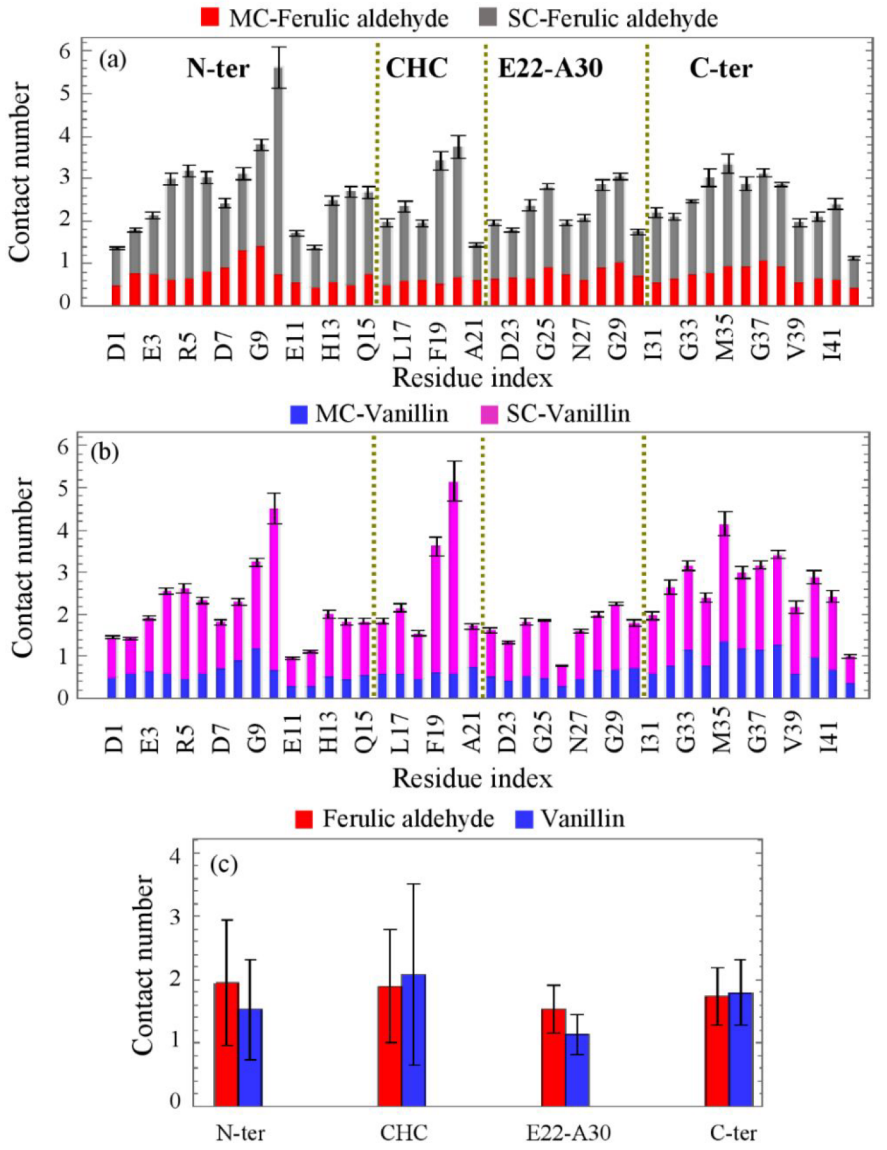

Figure 2. Average number of contacts between main-chain (MC)/side-chain (SC) of each residue in Aβ_{42} dimer and (a) ferulic aldehyde, (b) vanillin. (c) The averaged contact number for four different regions of Aβ peptide; N-terminus (N-ter), CHC, ^{22}EDVGSNKGA^{30} (E22-A30), and C-terminus (C-ter). The error bars represent the standard deviation of the mean. For panels a and b, the error bars correspond to the standard deviation of the mean of the cumulated MC and SC contacts. The dashed lines separate the different regions of Aβ (N-ter, CHC, E22-A30, and C-ter). The number of contacts were calculated for the cutoff distance of 0.5 nm.

study on the Aβ17−42 trimer and curcumin by Chebaro et al. demonstrated that curcumin preferentially interacts with the CHC region.[98] Moreover, solid-state NMR experiments suggested that the CHC segment is a possible binding site for curcumin.[59,65,99] Taken together, these results show that the curcumin compounds have a high propensity to interact with the CHC (Figure 2c) and, in particular, with its aromatic residues. Importantly, the ^{17}LVFF^{20} segment has been shown to play a central role in Aβ misfolding and aggregation.[87−93,97,100]

The contact map analysis reveals that the phenyl ring and the methoxy group (OCH3) in ferulic aldehyde interact more frequently with the residues in CHC region than vanillin (Figure 3a,b). Additionally, all groups of the ferulic aldehyde show a high contact probability with the N-terminus segment compared to these groups in vanillin, while in the presence of vanillin, all groups form more interactions with residues in the C-terminus region than ferulic aldehyde and, hence, could be a main factor in increase of the averaged contact numbers with this region (see Figure 2c and Figure 3b). The hydroxyl group (OH), methoxy group (OCH_3), and aldehyde group (CHO) in ferulic aldehyde and vanillin (Figure 3c,d) can interact with the Aβ dimer through the formation of hydrogen bonds and $\pi-\pi$ stacking with the Aβ_{42} dimer.

Effective Interactions in Aβ_{42} Dimer−Ligand Complex. The ligand−peptide hydrogen bond (H-bond) analysis shows that ferulic aldehyde forms the more frequent of H-bonds with residues Q15 and L34 than vanillin (Figure 4a,b). A similar observation was drawn by Zhao et al. in studying the effect of curcumin on the stability of Aβ dimers in which it was shown that curcumin predominantly interacts with residues Q15 and L34.[66] Apart from curcumin, epigallocatechin (EGC) exhibited high hydrogen bonding preference with residue Q15.[20] Compared to ferulic aldehyde, vanillin forms more H-

https://doi.org/10.1021/acs.jpcb.2c05846
J. Phys. Chem. B 2022, 126, 7627−7637

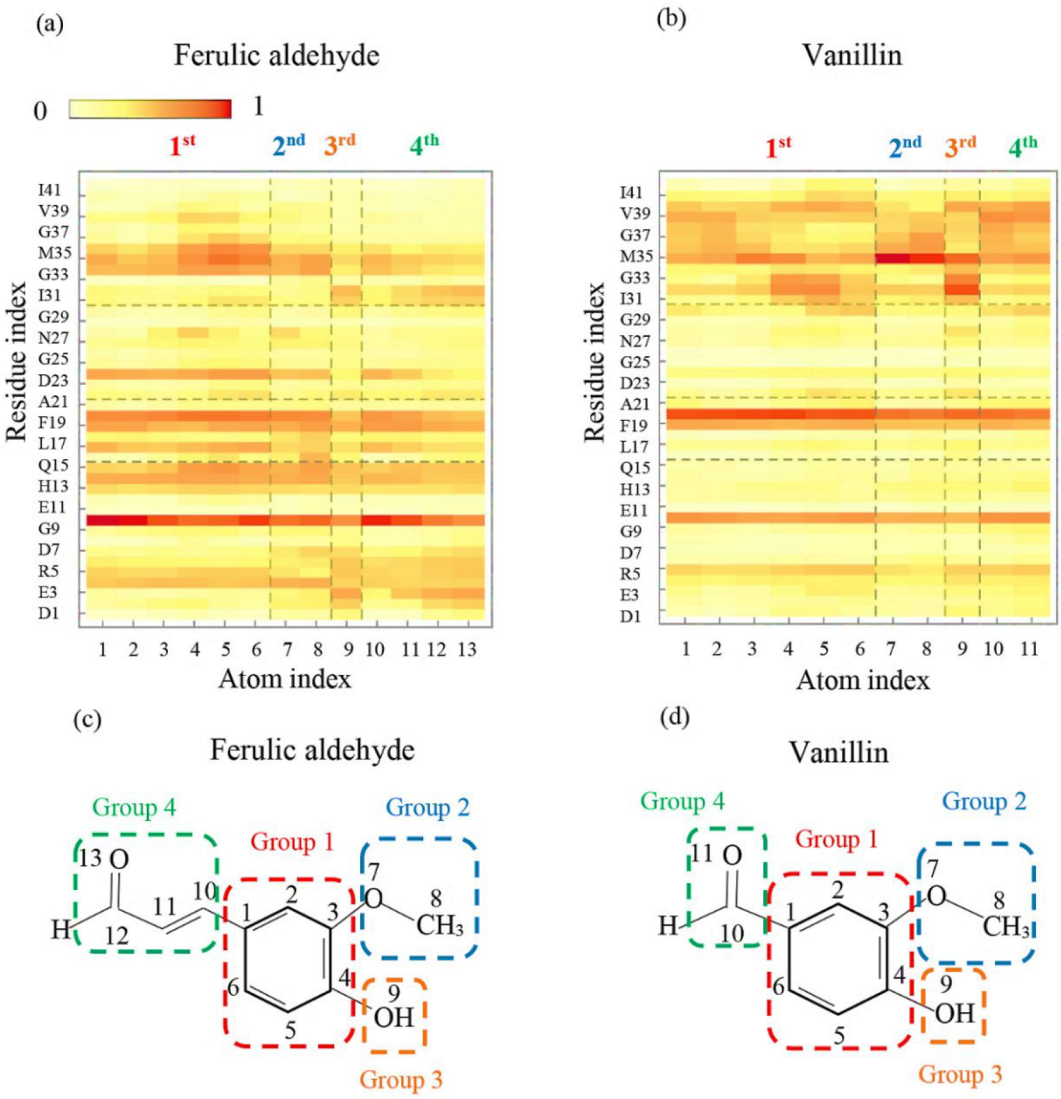

Figure 3. Contact map between the heavy atoms of Aβ_{42} residues and (a) ferulic aldehyde and (b) vanillin. (c, d) Structure of each ligand decomposed into four functional groups. The horizontal and vertical dashes correspond to the different regions of Aβ (N-terminus, CHC, ^{22}EDVGSNKGA^{30}, and C-terminus) and functional groups of each ligand, respectively. A contact is formed when the distance between the heavy atoms is less than 0.5 nm.

bonds with the ^{31}IIG^{33} and ^{40}VI^{41} sequences in the C-terminus region (Figure 4c). In fact, the strong interaction of vanillin with the C-terminal residues of the Aβ_{42} peptides results from the increased hydrogen bond contacts formed by its hydroxyl group (OH), methoxy group (OCH_3), and aldehyde group (CHO) with residues G33, V40, and I41.

Both ferulic aldehyde and vanillin interact with high propensity with residues Y10, F19, and F20 via $\pi-\pi$ stacking (Figure 5a). These observations are in line with the previous computational studies reporting that curcumin interacts with Aβ_{42} via $\pi-\pi$ stacking with the side-chains of F4, Y10, F19, and F20 in monomers and also H14 for Aβ in dimers and fibrils.[18,60,61,65,66,68] Furthermore, we examined the stacking pattern between each ligand ring and each aromatic residue by calculating the centroid distance and angle between the two rings (Figure 5b–d). Ferulic aldehyde prefers to form parallel $\pi-\pi$ stacking with Y10 and T-shaped $\pi-\pi$ stacking with F20 (Figure 5e,f). Vanillin forms T-shaped $\pi-\pi$ stacking with Y10 and parallel $\pi-\pi$ stacking with F20 (Figure 5g). Figure 5b,d shows that the parallel and T-shaped stacking patterns are the dominant packing modes for the aromatic residues with a high number of $\pi-\pi$ stacking interactions. From the H-bond and $\pi-\pi$ stacking analysis (Figures 4 and 5), we identify that ferulic aldehyde more effectively interacts with the dimer by the increasing the number of H-bonds formed by its hydroxyl group (OH), methoxy group (OCH_3), and aldehyde group (CHO) with the CHC and N-terminus segments and more $\pi-\pi$ stacking interactions with F4, H6, Y10, and H14 as compared to vanillin.

The Disruptive and Inhibitory Effects of Curcumin Products on the Aβ_{42} Dimer. The average C_α-RMSD values for the full length Aβ_{42} dimer and of four individual segments (N-terminus, CHC, ^{22}EDVGSNKGA^{30}, and C-terminus) show no significant differences in the presence of the small molecules (Figure 6a). To further characterize the effects of the degradation products of curcumin, we calculated the intramolecular salt-bridge populations (Figure 6b). First, we analyzed the salt-bridges identified from the known fibrillar

https://doi.org/10.1021/acs.jpcb.2c05846
J. Phys. Chem. B 2022, 126, 7627−7637

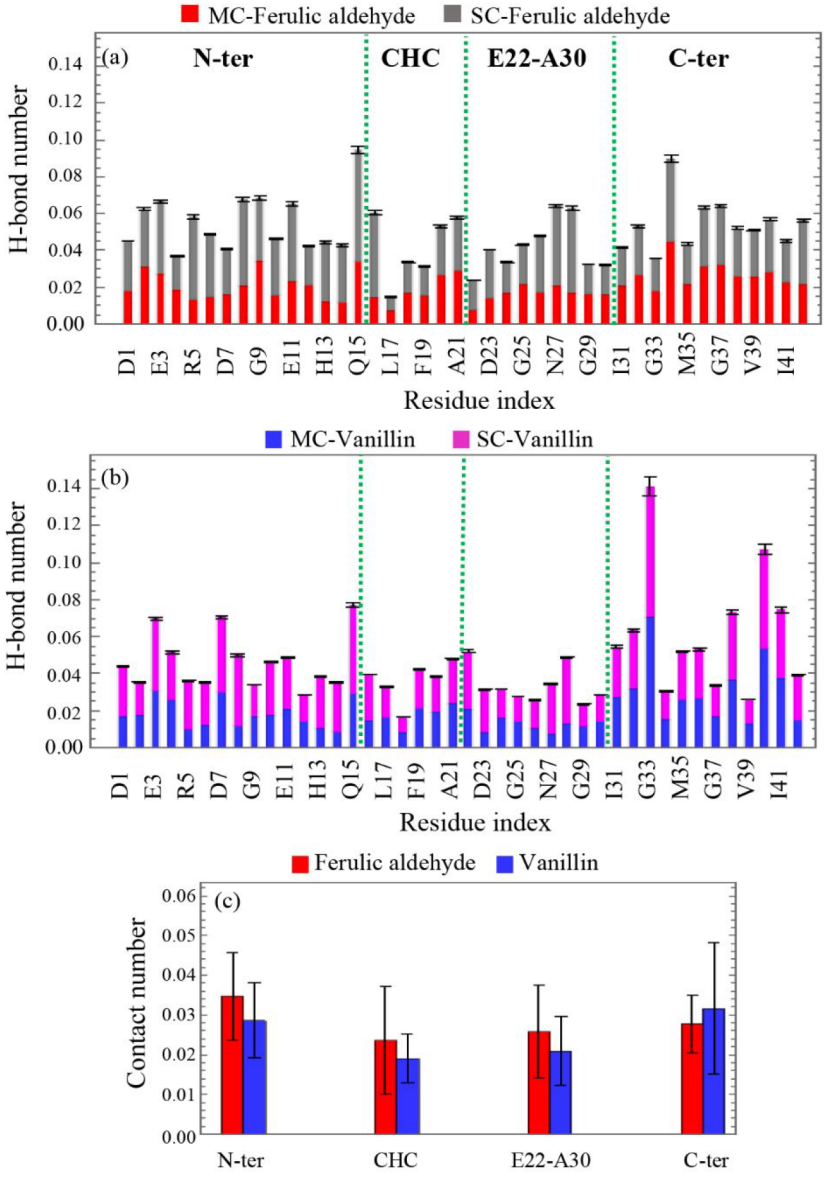

Figure 4. Average H-bond number between main-chain (MC)/side-chain (SC) of each residue in Aβ_{42} dimer and (a) ferulic aldehyde, (b) vanillin. (c) The averaged H-bond number for four different regions of Aβ peptide: N-terminus (N-ter), CHC, ^{22}EDVGSNKGA^{30} (E22-A30), and C-terminus (C-ter). An H-bond is formed if the acceptor−donor distance and acceptor−donor−hydrogen angle are less than 0.35 nm and 30°, respectively.[20] The error bars represent the standard deviation of the mean. The green dashed lines indicate the different regions of Aβ peptide: N-terminus (N-ter), CHC, ^{22}EDVGSNKGA^{30} (E22-A30), and C-terminus (C-ter).

structures of the peptide. The most recent cryo-electron microscopy structure of the full length Aβ_{42} fibril (LS-shape fibril structure; PDB id: 5OQV[101]) identified the intramolecular salt-bridges D7-R5, E11-H6 and E11-H13, and K28-A42.[101] Furthermore, the K28-A42 salt-bridge is present in the S-shaped Aβ_{11-42} (PDB id: 2MXU)[102] and Aβ_{15-42} (PDB id: 5KK3)[103] and also LS-shaped Aβ_{42} fibrils. Our simulations reveal that the D7-R5, E11-H6, E11-H13, and K28-A42 salt-bridges are only sporadically populated in the presence of the small molecules. On the other hand, we find that the small molecules have a more pronounced effect on other salt-bridges. For instance, ferulic aldehyde stimulates the formation of the D7-K28, E11-K28, and E22-K28 salt-bridges, while vanillin impacts predominantly the D7-K16, D7-K28, E11-H13, E11-K28, and D23-K28 contacts. Taken together, it is evident that the ligands have a different impact on the formation of the E22-K28 and D23-K28 salt-bridges.

CONCLUSIONS

Inhibition of the Aβ dimerization is a challenging task due to the intrinsic plasticity of the Aβ_{42} dimers. The structural heterogeneity and transient kinetics are a major obstacle for theoretical and experimental methods. To tackle this problem, several sampling methods have been proposed for constructing a representative conformational ensemble for Aβ. To this end, we have very recently employed the BES method for sampling of the Aβ_{42} dimers and shown that BES generated a heterogeneous conformational library of the Aβ_{42} dimers in good agreement with experimental data.[69] Here, we investigated the interaction between the Aβ_{42} dimers sampled by the BES protocol and two curcumin degradation products,

https://doi.org/10.1021/acs.jpcb.2c05846
J. Phys. Chem. B 2022, 126, 7627−7637

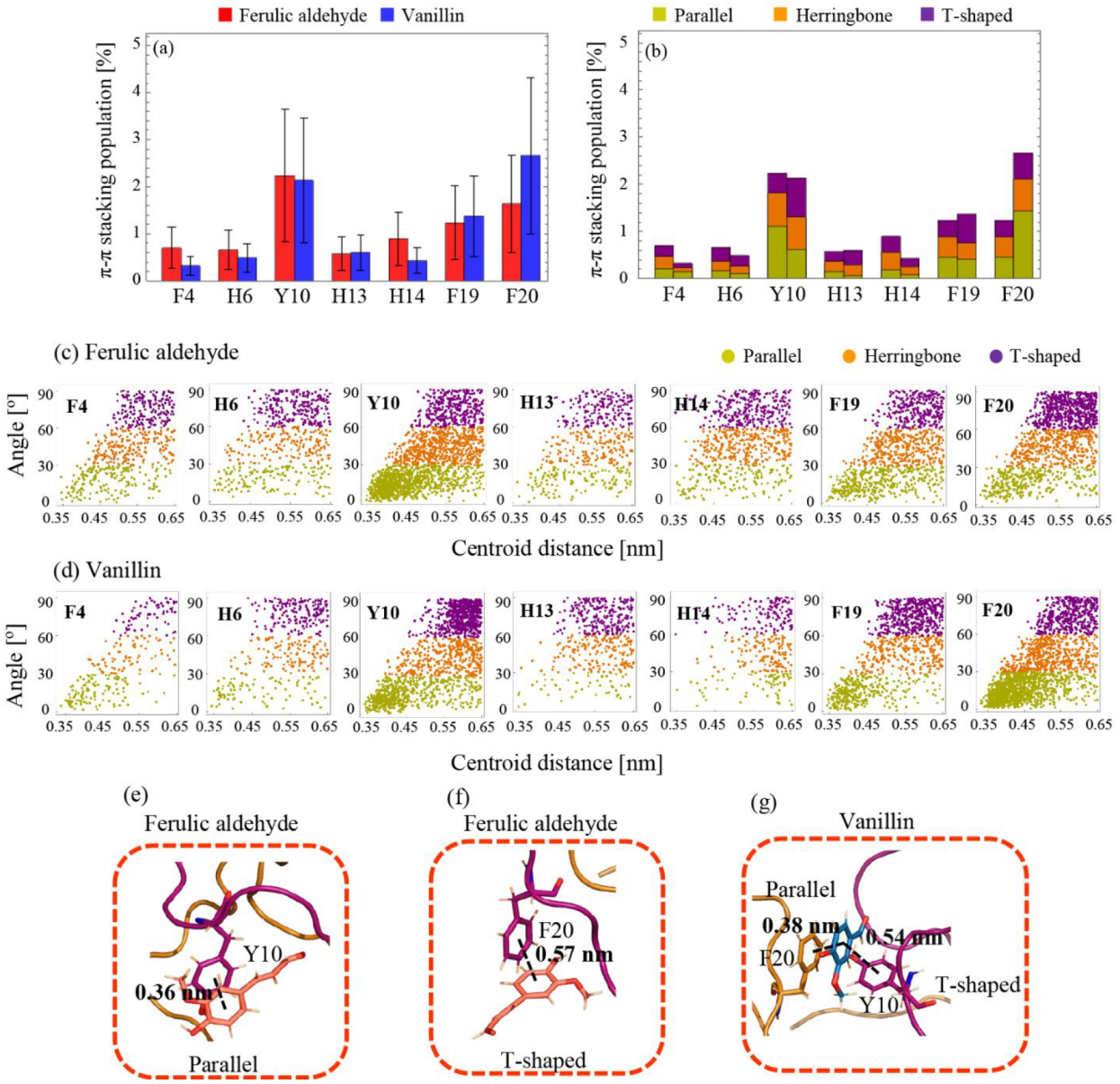

Figure 5. (a) The population (in %) of $\pi-\pi$ stacking between the phenyl ring of each ligand and aromatic residue within Aβ_{42} dimer. (b) The population (in %) of parallel, herringbone, and T-shaped stacking between the phenyl ring of each ligand and aromatic residue. Distributions of the centroid distance and angle between two phenyl rings of each aromatic residue and ligand. (c) Ferulic aldehyde and (d) vanillin. The $\pi-\pi$ interaction is formed if the centroid distance between two phenyl rings is less than 0.65 nm. The $\pi-\pi$ stacking patterns are classified into three categories: parallel (0−30°), herringbone (30−60°), and perpendicular or T-shaped (60−90°).[20] The $\pi-\pi$ stacking interactions were calculated by codes written with Mathematica software. Representative stacking patterns showing the parallel $\pi-\pi$ stacking between Y10 and ferulic aldehyde and T-shaped stacking pattern between F20 and ferulic aldehyde (e, f), T-shaped stacking between Y10 and vanillin and parallel stacking pattern between F20 and vanillin (g). The interacting aromatic residues in chainA and chainB are colored in purple and brown, respectively. $\pi-\pi$ interactions are given by black dashes. Ferulic aldehyde and vanillin are represented in stick with two colors, pink and blue, respectively.

ferulic aldehyde and vanillin, by ensemble docking and MD simulations (cumulative sampling of 2 μs).

Overall, the simulation results indicate that the curcumin products share the same binding "hot spot" (^{16}KLVFFA^{21}) on the Aβ_{42} dimer. Importantly, the interaction between the ^{16}KLVFFA^{21} regions in Aβ_{42} monomers is key for fibril formation and stabilization.[87−93] The contact number analysis provides evidence that ferulic aldehyde interacts with the Aβ_{42} dimer more effectively than vanillin. Ferulic aldehyde preferentially interacts with the N-terminus residues F4, Y10, H14, and also residues F19 and F20 in the CHC segment, whereas vanillin interacts with the Aβ_{42} dimer via $\pi-\pi$ stacking interactions with residues Y10, F19, and F20. Moreover, vanillin forms more hydrogen bond interactions with the C-terminus residues in the Aβ_{42} dimer than ferulic aldehyde.

The RMSD values calculated for each region of the Aβ_{42} dimer show that both ligands mainly affect the CHC region without dissociating the dimer. In the presence of ferulic aldehyde, one observes the small population of the intramolecular salt-bridges E11-H6 and K28-A42 that are important to stabilize the LS shape of the fibril structure. Furthermore, the E11-H13 salt-bridge is more stable in the presence of vanillin. On the basis of these results, ferulic aldehyde is predicted to be a more effective inhibitor of Aβ_{42} dimerization

https://doi.org/10.1021/acs.jpcb.2c05846
J. Phys. Chem. B 2022, 126, 7627−7637

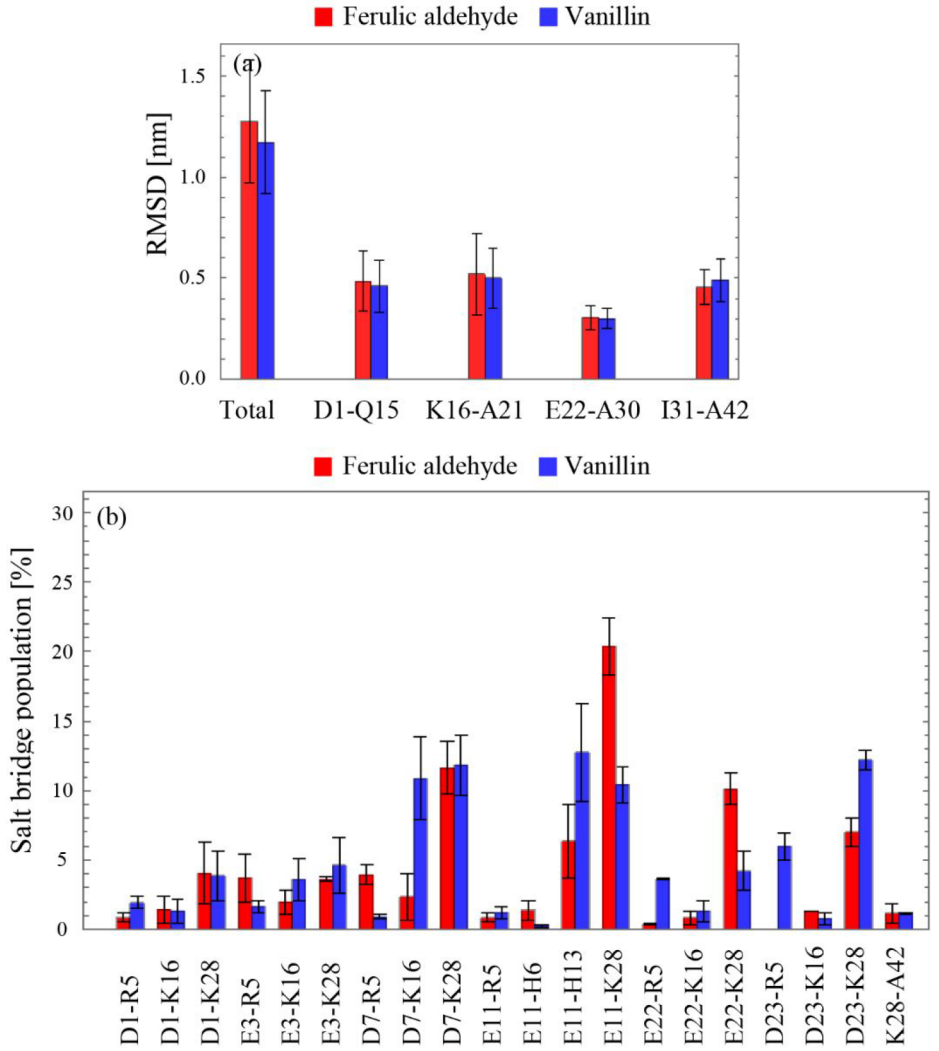

Figure 6. (a) The averaged and standard deviation of Cα-RMSD for the total and four regions (N-ter, CHC, E22-A30, and C-ter) in Aβ_{42} peptide in the presence of ferulic aldehyde and vanillin. (b) The population (in %) of intramolecular salt-bridges formed in Aβ_{42} dimer in the presence of ferulic aldehyde and vanillin as a ligand. The RMSD was calculated for the carbon alpha (Cα) as RMSD $= \sqrt{\frac{1}{N}\sum_{i=1}^{N}(r_i - r_i^{\mathrm{ref}})^2}$ where r_i^{ref} represents the reference position of atom i, and N shows the number of carbon atoms belonging to the total and each segment in the dimer. The error bars represent the standard deviation of the mean. A salt-bridge is formed when the minimum distance between the charged atoms is equal to or less than 0.35 nm.[104]

than vanillin. *In vivo* data shows that ferulic aldehyde effectively reduces the Aβ deposits and the toxic soluble Aβ oligomers, thus eliminating AD-like pathological changes in the hippocampus and cerebral cortex and improving the learning and memory capacity of the model mice.[105] Furthermore, both *in vitro* and *in vivo* studies show that vanillin and its derivatives have inhibitory potential against acetylcholinesterase, antioxidant properties, and amyloid-aggregation inhibitory effects.[55−57,106,107]

In conclusion, the degradation compounds of curcumin can inhibit the Aβ association by effective interactions with the aromatic residues ^{19}FF^{20} in the CHC region. The simulation results also reveal the presence of hydrogen bonds between the OH, OCH_3, and CHO groups on the phenyl rings of the degradation products and residues in the N-terminus and C-terminus of Aβ. This work sheds light on the influence of curcumin degradation products on the Aβ dimer, which may be beneficial for the design of drug candidates.

■ ASSOCIATED CONTENT

Supporting Information

The Supporting Information is available free of charge at https://pubs.acs.org/doi/10.1021/acs.jpcb.2c05846.

Histograms of binding affinity, plots of the minimum distance between each ligand and Aβ_{42} dimer structure, convergence of docking and molecular dynamics simulations, and the number of contacts between individual residues and each compound for different $\Delta\Delta G_{\mathrm{binding}}$ (PDF)

■ AUTHOR INFORMATION

Corresponding Authors

Ioana M. Ilie − *Van't Hoff Institute for Molecular Sciences, University of Amsterdam, 1098 XH Amsterdam, The Netherlands;* orcid.org/0000-0002-5935-3332; Email: i.m.ilie@uva.nl

https://doi.org/10.1021/acs.jpcb.2c05846
J. Phys. Chem. B 2022, 126, 7627−7637

Rohoullah Firouzi − *Department of Physical Chemistry, Chemistry and Chemical Engineering Research Center of Iran, 1496813151 Tehran, Iran;* orcid.org/0000-0003-2385-831X; Email: rfirouzi@ccerci.ac.ir, firouzi.chemist@yahoo.com

Authors

Maryam Haji Dehabadi − *Department of Physical Chemistry, Chemistry and Chemical Engineering Research Center of Iran, 1496813151 Tehran, Iran*

Amedeo Caflisch − *Department of Biochemistry, University of Zurich, CH-8057 Zurich, Switzerland;* orcid.org/0000-0002-2317-6792

Complete contact information is available at: https://pubs.acs.org/10.1021/acs.jpcb.2c05846

Author Contributions

A.C., I.M.I., and R.F. designed and directed the project. R.F. performed and analyzed the docking simulations. M.H.D. performed and analyzed the MD simulations. M.H.D prepared the manuscript. All authors discussed the results and reviewed the manuscript.

Notes

The authors declare no competing financial interest.

■ ACKNOWLEDGMENTS

The computational resources were provided by the Swiss National Supercomputing Centre (CSCS) in Lugano.

■ REFERENCES

(1) Ross, C. A.; Poirier, M. A. What is the role of protein aggregation in neurodegeneration? *Nat. Rev. Mol. Cell Biol.* **2005**, *6*, 891−898.
(2) Selkoe, D. J.; Hardy, J. The amyloid hypothesis of Alzheimer's disease at 25 years. *EMBO Mol. Med.* **2016**, *8*, 595−608.
(3) Prince, M. J.; Wimo, A.; Guerchet, M. M.; Ali, G. C.; Wu, Y. T.; Prina, M. *World Alzheimer Report 2015: The Global Impact of Dementia: An Analysis of Prevalence, Incidence, Cost and Trends*; Alzheimer's Disease International: London, 2015; p 84. http://www.alz.co.uk/research/world-report-2015 (accessed 2015-08).
(4) Reitz, C.; Brayne, C.; Mayeux, R. Epidemiology of Alzheimer disease. *Nat. Rev. Neurol.* **2011**, *7*, 137−152.
(5) Prince, M. J.; Comas-Herrera, A.; Knapp, M.; Guerchet, M.; Karagiannidou, M. *World Alzheimer Report 2016: Improving Healthcare for People Living with Dementia: Coverage, Quality and Costs Now and in the Future*; Alzheimer's Disease International: London, 2016; p 131. https://www.alz.co.uk/research/world-report-2016 (accessed 2016-09-21).
(6) Doig, A. J.; del Castillo-Frias, M. P.; Berthoumieu, O.; Tarus, B.; Nasica-Labouze, J.; Sterpone, F.; Nguyen, P. H.; Hooper, N. M.; Faller, P.; Derreumaux, P. Why is research on amyloid-β failing to give new drugs for Alzheimer's disease? *ACS Chem. Neurosci.* **2017**, *8*, 1435−1437.
(7) Serrano-Pozo, A.; Frosch, M. P.; Masliah, E.; Hyman, B. T. Neuropathological alterations in Alzheimer disease. *Cold Spring Harb. Perspect. Med.* **2011**, *1*, a006189.
(8) Kumar, A.; Singh, A. A review on Alzheimer's disease pathophysiology and its management: an update. *Pharmacol Rep.* **2015**, *67*, 195−203.
(9) Soto, C. Unfolding the role of protein misfolding in neurodegenerative diseases. *Nat. Rev. Neurosci.* **2003**, *4*, 49−60.
(10) Ilie, I. M.; Caflisch, A. Simulation studies of amyloidogenic polypeptides and their aggregates. *Chem. Rev.* **2019**, *119*, 6956−6993.
(11) Lomakin, A.; Teplow, D. B.; Kirschner, D. A.; Benedek, G. B. Kinetic theory of fibrillogenesis of amyloid-β protein. *Proc. Natl. Acad. Sci. U.S.A.* **1997**, *94*, 7942−7947.
(12) Hellstrand, E.; Boland, B.; Walsh, D. M.; Linse, S. Amyloid-β protein aggregation produces highly reproducible kinetic data and occurs by a two-phase process. *ACS Chem. Neurosci.* **2010**, *1*, 13−18.
(13) Rodrigues, T.; Reker, D.; Schneider, P.; Schneider, G. Counting on natural products for drug design. *Nat. Chem.* **2016**, *8*, 531−541.
(14) Henríquez, G.; Gomez, A.; Guerrero, E.; Narayan, M. Potential Role of Natural Polyphenols against Protein Aggregation Toxicity: In Vitro, In Vivo, and Clinical Studies. *ACS Chem. Neurosci.* **2020**, *11*, 2915−2934.
(15) Zheng, Q.; Kebede, M. T.; Kemeh, M. M.; Islam, S.; Lee, B.; Bleck, S. D.; Wurfl, L. A.; Lazo, N. D. Inhibition of the Self-Assembly of Aβ and of Tau by Polyphenols: Mechanistic Studies. *Molecules* **2019**, *24*, 2316.
(16) Nam, G.; Hong, M.; Lee, J.; Lee, H. J.; Ji, Y.; Kang, J.; Baik, M.-H.; Lim, M. H. Multiple reactivities of flavonoids towards pathological elements in Alzheimer's disease: structure−activity relationship. *Chem. Sci.* **2020**, *11*, 10243−10254.
(17) Ngo, S. T.; Li, M. S. Curcumin binds to Aβ1−40 peptides and fibrils stronger than ibuprofen and naproxen. *J. Phys. Chem. B* **2012**, *116*, 10165−10175.
(18) Rao, P. P.; Mohamed, T.; Teckwani, K.; Tin, G. Curcumin binding to beta amyloid: a computational study. *Chem. Biol. Drug Des.* **2015**, *86*, 813−820.
(19) Firouzi, R.; Sowlati-Hashjin, S.; Chávez-García, C.; Ashouri, M.; Karimi-Jafari, M. H.; Karttunen, M. Identification of Catechins Binding Pockets in Monomeric Aβ42 Through Ensemble Docking and MD Simulations. *BioRxiv* 2022, DOI: 10.1101/2022.02.09.479729.
(20) Zhan, C.; Chen, Y.; Tang, Y.; Wei, G. Green Tea Extracts EGCG and EGC Display Distinct Mechanisms in Disrupting Aβ_{42} Protofibril. *ACS Chem. Neurosci.* **2020**, *11*, 1841−1851.
(21) Gong, Y.; Zhan, C.; Zou, Y.; Qian, Z.; Wei, G.; Zhang, Q. Serotonin and Melatonin Show Different Modes of Action on Aβ_{42} Protofibril Destabilization. *ACS Chem. Neurosci.* **2021**, *12*, 799−809.
(22) Salamanova, E.; Atanasova, M.; Dimitrov, I.; Doytchinova, I. Effects of Curcumin and Ferulic Acid on the Folding of Amyloid-β Peptide. *Molecules* **2021**, *26*, 2815.
(23) Morales, I.; Cerda-Troncoso, C.; Andrade, V.; Maccioni, R. B. The natural product curcumin as a potential coadjuvant in Alzheimer's treatment. *J. Alzheimer's Dis.* **2017**, *60*, 451−460.
(24) Sevigny, J.; Chiao, P.; Bussière, T.; Weinreb, P. H.; Williams, L.; Maier, M.; Dunstan, R.; Salloway, S.; Chen, T.; Ling, Y.; et al. The antibody aducanumab reduces Aβ plaques in Alzheimer's disease. *Nature* **2016**, *537*, 50−56.
(25) Chen, M.; Du, Z. Y.; Zheng, X.; Li, D. L.; Zhou, R. P.; Zhang, K. Use of curcumin in diagnosis, prevention, and treatment of Alzheimer's disease. *Neural Regen. Res.* **2018**, *13*, 742−752.
(26) Wilken, R.; Veena, M. S.; Wang, M. B.; Srivatsan, E. S. Curcumin: a review of anti-cancer properties and therapeutic activity in head and neck squamous cell carcinoma. *Mol. Cancer* **2011**, *10*, 12.
(27) Miklossy, G.; Hilliard, T. S.; Turkson, J. Therapeutic modulators of STAT signalling for human diseases. *Nat. Rev. Drug Discovery* **2013**, *12*, 611−629.
(28) Zorofchian Moghadamtousi, S.; Abdul Kadir, H.; Hassandarvish, P.; Tajik, H.; Abubakar, S.; Zandi, K. A review of antibacterial, antiviral and antifungal activity of curcumin. *Bio. Med. Res.* **2014**, *2014*, 186864.
(29) Hamaguchi, T.; Ono, K.; Yamada, M. Curcumin and Alzheimer's disease. *CNS Neurosci. Ther.* **2010**, *16*, 285−297.
(30) Aggarwal, B. B.; Sung, B. Pharmacological basis for the role of curcumin in chronic diseases: an age-old spice with modern targets. *Trends Pharmacol. Sci.* **2009**, *30*, 85−94.
(31) Banerjee, R. Effect of curcumin on the metal ion induced fibrillization of amyloid-β peptide. *Spectrochim. Acta, Part A* **2014**, *117*, 798−800.
(32) Ono, K.; Hasegawa, K.; Naiki, H.; Yamada, M. Curcumin has potent anti-amyloidogenic effects for Alzheimer's amyloid-β fibrils *in vitro*. *J. Neurosci. Res.* **2004**, *75*, 742−750.

(33) Rane, J. S.; Bhaumik, P.; Panda, D. Curcumin inhibits tau aggregation and disintegrates preformed tau filaments *in vitro*. *J. Alzheimer's Dis.* **2017**, *60*, 999−1014.
(34) Ma, Q.-L.; Zuo, X.; Yang, F.; Ubeda, O. J.; Gant, D. J.; Alaverdyan, M.; Teng, E.; Hu, S.; Chen, P.-P.; Maiti, P. Curcumin suppresses soluble tau dimers and corrects molecular chaperone, synaptic, and behavioral deficits in aged human tau transgenic mice. *J. Biol. Chem.* **2013**, *288*, 4056−4065.
(35) Yang, F.; Lim, G. P.; Begum, A. N.; Ubeda, O. J.; Simmons, M. R.; Ambegaokar, S. S.; Chen, P. P.; Kayed, R.; Glabe, C. G.; Frautschy, S. A. Curcumin inhibits formation of amyloid-β oligomers and fibrils, binds plaques, and reduces amyloid *in vivo*. *J. Biol. Chem.* **2005**, *280*, 5892−5901.
(36) Yanagisawa, D.; Ibrahim, N. F.; Taguchi, H.; Morikawa, S.; Hirao, K.; Shirai, N.; Sogabe, T.; Tooyama, I. Curcumin derivative with the substitution at C-4 position, but not curcumin, is effective against amyloid pathology in APP/PS1 mice. *Neurobiol. Aging* **2015**, *36*, 201−210.
(37) Yanagisawa, D.; Taguchi, H.; Yamamoto, A.; Shirai, N.; Hirao, K.; Tooyama, I. Curcuminoid binds to amyloid-β(1−42) oligomer and fibril. *J. Alzheimer's Dis.* **2011**, *24*, 33−42.
(38) Thapa, A.; Jett, S. D.; Chi, E. Y. Curcumin attenuates amyloid-β aggregate toxicity and modulates amyloid-β aggregation pathway. *ACS Chem. Neurosci.* **2016**, *7*, 56−68.
(39) Wang, Y.-J.; Pan, M.-H.; Cheng, A.-L.; Lin, L.-I.; Ho, Y.-S.; Hsieh, C.-Y.; Lin, J.-K. Stability of curcumin in buffer solutions and characterization of its degradation products. *J. Pharm. Biomed. Anal.* **1997**, *15*, 1867−1876.
(40) Cox, K. H.; Pipingas, A.; Scholey, A. B. Investigation of the effects of solid lipid curcumin on cognition and mood in a healthy older population. *J. Psychopharmacol.* **2015**, *29*, 642−651.
(41) Small, G. W.; Siddarth, P.; Li, Z.; Miller, K. J.; Ercoli, L.; Emerson, N. D.; Martinez, J.; Wong, K.-P.; Liu, J.; Merrill, D. A. Memory and brain amyloid and tau effects of a bioavailable form of curcumin in non-demented adults: a double-blind, placebo-controlled 18-month trial. *Am. J. Geriatr. Psychiatry* **2018**, *26*, 266−277.
(42) Heger, M.; van Golen, R. F.; Broekgaarden, M.; Michel, M. C. The molecular basis for the pharmacokinetics and pharmacodynamics of curcumin and its metabolites in relation to cancer. *Pharmacol. Rev.* **2014**, *66*, 222−307.
(43) Anand, P.; Kunnumakkara, A. B.; Newman, R. A.; Aggarwal, B. B. Bioavailability of curcumin: problems and promises. *Mol. Pharmaceutics* **2007**, *4*, 807−818.
(44) Tsuda, T. Curcumin as a functional food-derived factor: degradation products, metabolites, bioactivity, and future perspectives. *Food Funct.* **2018**, *9*, 705−714.
(45) Shen, L.; Liu, C. C.; An, C. Y.; Ji, H. F. How does curcumin work with poor bioavailability? Clues from experimental and theoretical studies. *Sci. Rep.* **2016**, *6*, 20872.
(46) Shen, L.; Ji, H.-F. The pharmacology of curcumin: is it the degradation products? *Trends Mol. Med.* **2012**, *18*, 138−144.
(47) Gordon, O. N.; Schneider, C. Vanillin and ferulic acid: not the major degradation products of curcumin. *Trends Mol. Med.* **2012**, *18*, 361−363.
(48) Sultana, R.; Ravagna, A.; Mohmmad-Abdul, H.; Calabrese, V.; Butterfield, D. A. Ferulic acid ethyl ester protects neurons against amyloid-β(1−42) peptide-induced oxidative stress and neurotoxicity: relationship to antioxidant activity. *J. Neurochem.* **2005**, *92*, 749−758.
(49) Srinivasan, M.; Sudheer, A. R.; Menon, V. P. Ferulic acid: therapeutic potential through its antioxidant property. *J. Clin. Biochem. Nutr.* **2007**, *40*, 92−100.
(50) Kanski, J.; Aksenova, M.; Stoyanova, A.; Butterfield, D. A. Ferulic acid antioxidant protection against hydroxyl and peroxyl radical oxidation in synaptosomal and neuronal cell culture systems *in vitro*: structure-activity studies. *J. Nutr. Biochem.* **2002**, *13*, 273−281.
(51) Phadke, A. V.; Tayade, A. A.; Khambete, M. P. Therapeutic potential of ferulic acid and its derivatives in Alzheimer's disease—A systematic review. *Chem. Biol. Drug Des.* **2021**, *98*, 713−721.
(52) Turkez, H.; Arslan, M. E.; Barboza, J. N.; Kahraman, C. Y.; de Sousa, D. P.; Mardinoğlu, A. Therapeutic Potential of Ferulic Acid in Alzheimer's Disease. *Curr. Drug Delivery* **2022**, *19*, 860−873.
(53) Singh, Y. P.; Rai, H.; Singh, G.; Singh, G. K.; Mishra, S.; Kumar, S.; Srikrishna, S.; Modi, G. A. review on ferulic acid and analogs based scaffolds for the management of Alzheimer's disease. *Eur. J. Med. Chem.* **2021**, *215*, 113278.
(54) Ono, K.; Hirohata, M.; Yamada, M. Ferulic acid destabilizes preformed β-amyloid fibrils *in vitro*. *Biochem. Biophys. Res. Commun.* **2005**, *336*, 444−449.
(55) Kundu, A.; Mitra, A. Flavoring extracts of Hemidesmus indicus roots and Vanilla planifolia pods exhibit *in vitro* acetylcholinesterase inhibitory activities. *Plant Foods Hum. Nutr.* **2013**, *68*, 247−253.
(56) Iannuzzi, C.; Borriello, M.; Irace, G.; Cammarota, M.; Di Maro, A.; Sirangelo, I. Vanillin affects amyloid aggregation and non-enzymatic glycation in human insulin. *Sci. Rep.* **2017**, *7*, 15086−14.
(57) Blaikie, L.; Kay, G.; Lin, P. K. T. Synthesis and *in vitro* evaluation of vanillin derivatives as multi-target therapeutics for the treatment of Alzheimer's disease. *Bioorg. Med. Chem. Lett.* **2020**, *30*, 127505.
(58) Ahmadi, N.; Safari, S.; Mirazi, N.; Karimi, S. A.; Komaki, A. Effects of vanillic acid on Aβ_{1-40}-induced oxidative stress and learning and memory deficit in male rats. *Brain Res. Bull.* **2021**, *170*, 264−273.
(59) Amin, F. U.; Shah, S. A.; Kim, M. O. Vanillic acid attenuates Aβ_{42}-induced oxidative stress and cognitive impairment in mice. *Sci. Rep.* **2017**, *7*, 40753.
(60) Jakubowski, J. M.; Orr, A. A.; Le, D. A.; Tamamis, P. Interactions between Curcumin Derivatives and Amyloid-β Fibrils: Insights from Molecular Dynamics Simulations. *J. Chem. Inf. Model.* **2020**, *60*, 289−305.
(61) Doytchinova, I.; Atanasova, M.; Salamanova, E.; Ivanov, S.; Dimitrov, I. Curcumin Inhibits the Primary Nucleation of Amyloid-Beta Peptide: A Molecular Dynamics Study. *Biomolecules* **2020**, *10*, 1323.
(62) Tavanti, F.; Pedone, A.; Menziani, M. C. Computational insight into the effect of natural compounds on the destabilization of preformed amyloid-β (1−40) fibrils. *Molecules* **2018**, *23*, 1320.
(63) Kundaikar, H. S.; Degani, M. S. Insights into the Interaction mechanism of ligands with Aβ42 based on molecular dynamics simulations and mechanics: implications of role of common binding site in drug design for alzheimer's disease. *Chem. Biol. Drug Des.* **2015**, *86*, 805−812.
(64) Bajda, M.; Filipek, S. Computational approach for the assessment of inhibitory potency against beta-amyloid aggregation. *Bioorg. Med. Chem. Lett.* **2017**, *27*, 212−216.
(65) Battisti, A.; Piccionello, A. P.; Sgarbossa, A.; Vilasi, S.; Ricci, C.; Ghetti, F.; Spinozzi, F.; Gammazza, A. M.; Giacalone, V.; Martorana, A. Curcumin-like compounds designed to modify amyloid beta peptide aggregation patterns. *RSC Adv.* **2017**, *7*, 31714−31724.
(66) Zhao, L. N.; Chiu, S.-W.; Benoit, J. r. m.; Chew, L. Y.; Mu, Y. The effect of curcumin on the stability of Aβ dimers. *J. Phys. Chem. B* **2012**, *116*, 7428−7435.
(67) Awasthi, M.; Singh, S.; Pandey, V. P.; Dwivedi, U. N. Modulation in the conformational and stability attributes of the Alzheimer's disease associated amyloid-beta mutants and their favorable stabilization by curcumin: Molecular dynamics simulation analysis. *J. Biomol. Struct. Dyn.* **2018**, *36*, 407−422.
(68) Zhu, M.; De Simone, A.; Schenk, D.; Toth, G.; Dobson, C. M.; Vendruscolo, M. Identification of small-molecule binding pockets in the soluble monomeric form of the Aβ_{42} peptide. *J. Chem. Phys.* **2013**, *139*, 035101.
(69) Dehabadi, M. H.; Firouzi, R. Constructing conformational library for amyloid-β42 dimers as the smallest toxic oligomers using two CHARMM force fields. *J. Mol. Graph. Model.* **2022**, *115*, 108207.
(70) Salehi, N.; Amininasab, M.; Firouzi, R.; Karimi-Jafari, M. H. Efficient construction of a diverse conformational library for amyloid-β as an intrinsically disordered protein. *J. Mol. Graph. Model.* **2019**, *88*, 183−193.

https://doi.org/10.1021/acs.jpcb.2c05846
J. Phys. Chem. B 2022, 126, 7627−7637

(71) Daura, X.; Gademann, K.; Jaun, B.; Seebach, D.; Van Gunsteren, W. F.; Mark, A. E. Peptide folding: when simulation meets experiment. *Angew. Chem., Int. Ed.* **1999**, *38*, 236−240.
(72) Bernstein, S. L.; Dupuis, N. F.; Lazo, N. D.; Wyttenbach, T.; Condron, M. M.; Bitan, G.; Teplow, D. B.; Shea, J.-E.; Ruotolo, B. T.; Robinson, C. V. Amyloid-β protein oligomerization and the importance of tetramers and dodecamers in the aetiology of Alzheimer's disease. *Nat. Chem.* **2009**, *1*, 326−331.
(73) Berendsen, H. J.; van der Spoel, D.; van Drunen, R. GROMACS: a message-passing parallel molecular dynamics implementation. *Comput. Phys. Commun.* **1995**, *91*, 43−56.
(74) Hess, B.; Kutzner, C.; Van Der Spoel, D.; Lindahl, E. GROMACS 4: algorithms for highly efficient, load-balanced, and scalable molecular simulation. *J. Chem. Theory Compu.* **2008**, *4*, 435−447.
(75) Huang, J.; Rauscher, S.; Nawrocki, G.; Ran, T.; Feig, M.; De Groot, B. L.; Grubmüller, H.; MacKerell, A. D. CHARMM36m: an improved force field for folded and intrinsically disordered proteins. *Nat. Methods* **2017**, *14*, 71−73.
(76) Onufriev, A.; Bashford, D.; Case, D. A. Exploring protein native states and large-scale conformational changes with a modified generalized born model. *Proteins* **2004**, *55*, 383−394.
(77) Irwin, J. J.; Shoichet, B. K. ZINC a free database of commercially available compounds for virtual screening. *J. Chem. Inf. Model.* **2005**, *45*, 177−182.
(78) Schmidt, M. W.; Baldridge, K. K.; Boatz, J. A.; Elbert, S. T.; Gordon, M. S.; Jensen, J. H.; Koseki, S.; Matsunaga, N.; Nguyen, K. A.; Su, S. General atomic and molecular electronic structure system. *J. Comput. Chem.* **1993**, *14*, 1347−1363.
(79) Stephens, P. J.; Devlin, F. J.; Chabalowski, C. F.; Frisch, M. J. Ab initio calculation of vibrational absorption and circular dichroism spectra using density functional force fields. *J. Phys. Chem.* **1994**, *98*, 11623−11627.
(80) Trott, O.; Olson, A. J. AutoDock Vina: improving the speed and accuracy of docking with a new scoring function, efficient optimization, and multithreading. *J. Comput. Chem.* **2010**, *31*, 455−461.
(81) Vanommeslaeghe, K.; Hatcher, E.; Acharya, C.; Kundu, S.; Zhong, S.; Shim, J.; Darian, E.; Guvench, O.; Lopes, P.; Vorobyov, I. CHARMM general force field: A force field for drug-like molecules compatible with the CHARMM all-atom additive biological force fields. *J. Comput. Chem.* **2010**, *31*, 671−690.
(82) Jorgensen, W. L.; Chandrasekhar, J.; Madura, J. D.; Impey, R. W.; Klein, M. L. Comparison of simple potential functions for simulating liquid water. *J. Chem. Phys.* **1983**, *79*, 926−935.
(83) Bussi, G.; Donadio, D.; Parrinello, M. Canonical sampling through velocity rescaling. *J. Chem. Phys.* **2007**, *126*, 014101.
(84) Berendsen, H. J.; Postma, J. v.; van Gunsteren, W. F.; DiNola, A.; Haak, J. R. Molecular dynamics with coupling to an external bath. *J. Chem. Phys.* **1984**, *81*, 3684−3690.
(85) Darden, T.; York, D.; Pedersen, L. Particle mesh Ewald: An N·log (N) method for Ewald sums in large systems. *J. Chem. Phys.* **1993**, *98*, 10089−10092.
(86) Masuda, Y.; Fukuchi, M.; Yatagawa, T.; Tada, M.; Takeda, K.; Irie, K.; Akagi, K.-i.; Monobe, Y.; Imazawa, T.; Takegoshi, K. Solid-state NMR analysis of interaction sites of curcumin and 42-residue amyloid β-protein fibrils. *Bioorg. Med. Chem.* **2011**, *19*, 5967−5974.
(87) Liu, R.; McAllister, C.; Lyubchenko, Y.; Sierks, M. R. Residues 17−20 and 30−35 of amyloid-β play critical roles in aggregation. *J. Neurosci. Res.* **2004**, *75*, 162−171.
(88) De Groot, N. S.; Aviles, F. X.; Vendrell, J.; Ventura, S. Mutagenesis of the central hydrophobic cluster in Aβ_{42} Alzheimer's peptide: Side-chain properties correlate with aggregation propensities. *FEBS J.* **2006**, *273*, 658−668.
(89) Chimon, S.; Shaibat, M. A.; Jones, C. R.; Calero, D. C.; Aizezi, B.; Ishii, Y. Evidence of fibril-like β-sheet structures in a neurotoxic amyloid intermediate of Alzheimer's amyloid-β. *Nat. Struct. Mol. Biol.* **2007**, *14*, 1157−1164.
(90) Härd, T.; Lendel, C. Inhibition of amyloid formation. *J. Mol. Biol.* **2012**, *421*, 441−465.
(91) Riek, R.; Eisenberg, D. S. The activities of amyloids from a structural perspective. *Nature* **2016**, *539*, 227−235.
(92) Nie, Q.; Du, X.-g.; Geng, M.-y Ligand inhibitors of amyloid-β peptide aggregation as a potential therapeutic strategy for Alzheimer's disease. *Acta Pharmacol. Sin.* **2011**, *32*, 545−551.
(93) Ilie, I. M.; Caflisch, A. Disorder at the tips of a disease-relevant Aβ42 amyloid fibril: A molecular dynamics study. *J. Phys. Chem. B* **2018**, *122*, 11072−11082.
(94) Huang, D.; Zimmerman, M. I.; Martin, P. K.; Nix, A. J.; Rosenberry, T. L.; Paravastu, A. K. Antiparallel β-sheet structure within the C-terminal region of 42-residue Alzheimer's Amyloid-β peptides when they form 150-KDa oligomers. *J. Mol. Biol.* **2015**, *427*, 2319−2328.
(95) Schmidt, M.; Rohou, A.; Lasker, K.; Yadav, J. K.; Schiene-Fischer, C.; Fändrich, M.; Grigorieff, N. Peptide dimer structure in an Aβ (1−42) fibril visualized with Cryo-EM. *Proc. Natl. Acad. Sci. U. S. A.* **2015**, *112*, 11858−11863.
(96) Pike, C. J.; Walencewicz-Wasserman, A. J.; Kosmoski, J.; Cribbs, D. H.; Glabe, C. G.; Cotman, C. W. Structure-activity analyses of beta-amyloid peptides: contributions of the beta 25−35 region to aggregation and neurotoxicity. *J. Neurochem.* **1995**, *64*, 253−265.
(97) Firouzi, R.; Noohi, B. Identification of key stabilizing interactions of amyloid-β oligomers based on fragment molecular orbital calculations on macrocyclic β-hairpin peptides. *Proteins* **2022**, *90*, 229−238.
(98) Chebaro, Y.; Jiang, P.; Zang, T.; Mu, Y.; Nguyen, P. H.; Mousseau, N.; Derreumaux, P. Structures of Aβ17−42 trimers in isolation and with five small-molecule drugs using a hierarchical computational procedure. *J. Phys. Chem. B* **2012**, *116*, 8412−8422.
(99) Hess, B.; Bekker, H.; Berendsen, H. J.; Fraaije, J. G. LINCS: a linear constraint solver for molecular simulations. *J. Comput. Chem.* **1997**, *18*, 1463−1472.
(100) Nguyen, P. H.; Ramamoorthy, A.; Sahoo, B. R.; Zheng, J.; Faller, P.; Straub, J. E.; Dominguez, L.; Shea, J.-E.; Dokholyan, N. V.; De Simone, A.; et al. Amyloid oligomers: A joint experimental/computational perspective on Alzheimer's disease, Parkinson's disease, type II diabetes, and amyotrophic lateral sclerosis. *Chem. Rev.* **2021**, *121*, 2545−2647.
(101) Gremer, L.; Schölzel, D.; Schenk, C.; Reinartz, E.; Labahn, J.; Ravelli, R. B.; Tusche, M.; Lopez-Iglesias, C.; Hoyer, W.; Heise, H. Fibril structure of amyloid-β(1−42) by cryo−electron microscopy. *Science* **2017**, *358*, 116−119.
(102) Xiao, Y.; Ma, B.; McElheny, D.; Parthasarathy, S.; Long, F.; Hoshi, M.; Nussinov, R.; Ishii, Y. Aβ(1−42) fibril structure illuminates self-recognition and replication of amyloid in Alzheimer's disease. *Nat. Struct. Mol. Biol.* **2015**, *22*, 499−505.
(103) Colvin, M. T.; Silvers, R.; Ni, Q. Z.; Can, T. V.; Sergeyev, I.; Rosay, M.; Donovan, K. J.; Michael, B.; Wall, J.; Linse, S. Atomic resolution structure of monomorphic Aβ_{42} amyloid fibrils. *J. Am. Chem. Soc.* **2016**, *138*, 9663−9674.
(104) Lemkul, J. A.; Huang, J.; MacKerell, A. D., Jr Induced dipole−dipole interactions influence the unfolding pathways of wild-type and mutant amyloid-β peptides. *J. Phys. Chem. B* **2015**, *119*, 15574−15582.
(105) Dong, Y.; Stewart, T.; Bai, L.; Li, X.; Xu, T.; Iliff, J.; Shi, M.; Zheng, D.; Yuan, L.; Wei, T.; Yang, X.; Zhang, J. Coniferaldehyde attenuates Alzheimer's pathology via activation of Nrf2 and its targets. *Theranostics* **2020**, *10*, 179.
(106) Scipioni, M.; Kay, G.; Megson, I.; Lin, P. K. T. Novel vanillin derivatives: Synthesis, anti-oxidant, DNA and cellular protection properties. *Eur. J. Med. Chem.* **2018**, *143*, 745−754.
(107) Scipioni, M.; Kay, G.; Megson, I. L.; Lin, P. K. T. Synthesis of novel vanillin derivatives: novel multi-targeted scaffold ligands against Alzheimer's disease. *MedChemComm* **2019**, *10*, 764−777.

https://doi.org/10.1021/acs.jpcb.2c05846
J. Phys. Chem. B 2022, 126, 7627−7637